IEEE Access
Multidisciplinary | Rapid Review | Open Access Journal

Received July 30, 2019, accepted August 2, 2019, date of publication August 12, 2019, date of current version August 26, 2019.

Digital Object Identifier 10.1109/ACCESS.2019.2934564

Adaptive Re-weighted Block Adjustment for Multi-Coverage Satellite Stereo Images without Ground Control Points

KUNBO LIU[1], PENGJIE TAO[1], KAI TAN[2], YANSONG DUAN[1], JIANAN HE[1], AND XIANGYONG LUO[3]

[1]School of Remote Sensing and Information Engineering, Wuhan University, Wuhan 430079, China
[2]State Key Laboratory of Estuarine and Coastal Research, East China Normal University, Shanghai 200241, China
[3]Key Laboratory for Aerial Remote Sensing Technology of Ministry of Natural Resources of the People's Republic of China, Beijing 100039, China

Corresponding author: Pengjie Tao (pjtao@whu.edu.cn)

This work was supported in part by the National Key Research and Development Program of China under Grant 2018YFD1100405.

ABSTRACT Georeferencing satellite imagery is the basis for mapping and other subsequent processing in photogrammetry and remote sensing. Traditional georeferencing methods, which require adequate and well-distributed ground control points (GCPs), are time-consuming, costly, constantly cumbersome and inefficient. This study proposes a method of adaptive re-weighted block adjustment without GCPs for satellite stereo images. Furthermore, an approach of using multi-coverage images to improve the direct georeferencing accuracy is also investigated. The bias-compensated rational function model with affine transformation parameters is used as the adjustment mathematical model. The ''weighted virtual control points'' are introduced as constraints in the adjustment. Space intersection and resection are executed iteratively to solve the accurate affine transformation parameters. A total of 722 three-line array stereo scenes of Chinese Mapping Satellite-1 images captured from December 2010 to March 2016, which cover the entire Shandong Province of China (about 158,000 km^2) nearly 10 times in space, are used as experimental data to evaluate the performance of the proposed method. Experiment results demonstrate that the proposed method can effectively eliminate the systematic errors of images. Moreover, the additional comparison with experiments of three groups of mono-coverage images indicates that the redundant observations from multi-coverage images can significantly improve the direct georeferencing accuracy, more specifically, from 13.69-16.02 m to 11.09 m in the horizontal direction, and from 16.39-29.27 m to 8.47 m in the vertical direction.

INDEX TERMS Georeferencing satellite imagery, block adjustment, without ground control points (GCPs), multi-coverage satellite images, weighted virtual control points.

I. INTRODUCTION

Satellites have the advantages of large scanning range, strong continuity, short revisit period, and stable orbital parameters, over other remote sensing platforms, such as aerial aircraft, unmanned aircraft, and vehicle cameras. Thus, satellites have attracted extensive attention in many large-scale photogrammetry applications. However, the initial orientation parameters of satellite images contain errors rising from the on-orbit calibration error of the satellite imaging sensor, the measurement errors of the positioning and attitude sensors, and the errors caused by the time asynchronous of different subsystems when acquiring data. Consequently, block adjustment is necessary to reduce or even eliminate the errors before subsequent processings.

The conventional methods use ground control points (GCPs) [1]–[3] or ground control lines (GCLs) [4]–[5] to perform block adjustment, thereby achieving the goal of eliminating the errors of the sensor model and data. These methods can achieve high geopositional accuracy, but the amount of required GCPs depends on the terrain complexity and directly influences the geopositional accuracy [6], [7]. A large coverage area or a complex terrain often requires numerous GCPs. However, GCP field measurement work is time-consuming, costly, and cannot be performed well in some extreme areas, such as deserts. Moreover, measuring

The associate editor coordinating the review of this article and approving it for publication was Bora Onat.

the observations of GCPs in multi-view images is constantly cumbersome and inefficient. These factors make block adjustment methods based on GCPs hard to perform in large-scale mapping works. Fortunately, with the development of satellite hardware, the accuracies of global positioning system (GPS) and attitude control sensors for measuring satellite orbit and attitude have been improved. These improvements provide high-precision exterior orientation elements for satellite images, thus reduces the errors in images. Currently, some satellites with high-precision orbit and attitude parameters achieve high direct geopositional accuracies using only space intersection [8] with stereo scenes. For example, the direct geopositional accuracy of WorldView-1 stereo images without GCPs is within 2 m in root mean square error (RMSE), and from which digital elevation model (DEM) with vertical error smaller than 5 m can be obtained [9]–[10]. Obviously, it is an inevitable trend to study geometric correction methods without GCPs, which can also achieve high geopositional accuracy.

An effective geometric correction technique without GCPs frequently makes a good use of existing geo-referenced data [11] as constraints in block adjustment, including oriented images with precise interior and exterior orientation parameters [12], [13], shuttle radar topography mission (SRTM) derived DEM [14]–[16], and geocoded images [17], [18]. However, the accuracies of these methods heavily rely on the reference data. In other words, these methods may be infeasible when the accuracy of the reference data is low or high-precision reference data is unavailable. Therefore, methods that only require initial high-precision external orientation parameters (EOPs) and other metadata are investigated. Reference [19] uses a hybrid model based on 3D deterministic Toutin's model, which exploits the image's metadata, to geometrically process WorldView-1 and WorldView-2 stereo images without GCPs; this model has achieved a vertical accuracy of 2.5 m over bare surfaces. A combined block adjustment approach [20] is proposed to integrate multi-source and multi-resolution satellite images for improving geopositional accuracy without GCPs; experiments demonstrated that this method can effectively improve the geopositional accuracies of satellite images using ZiYuan-3, SPOT-7, and Pleiades-1 images in Hong Kong and Cartosat-1 and WorldView-1 images in Catalonia, Spain. A new physical inverse model based on a double-iterative method, considering velocity aberration, optical path delay, and atmospheric refraction, is introduced in [21]. It achieves a horizontal accuracy of 3.8 m of WorldView-2 images, which is higher than the original geopositional accuracy using the original rational polynomial coefficients (RPCs) under the condition without any control data. In addition, many other studies on geometric correction technique without GCPs, such as direct georeferencing approach [22], and multi-trip bundle block adjustment method [23], have been conducted.

However, these methods list all the observations together in the error equations and perform the bundle (block) adjustment to solve the unknowns, thereby requiring considerable computational memory. Therefore, they are limited by the number and overlap of images and not conducive to parallel computing. Moreover, these methods treat all the image pairs as equal weight observations, which is not the case in actual production (the errors of the image pairs usually vary significantly) and thus possibly affects the accuracy of block adjustment. Therefore, in this paper, we propose an adaptive re-weighted block adjustment method without GCPs, which uses ''weighted virtual control points'' [24] as constraints instead of GCPs.

A short revisit period of satellites denotes that the same area of the earth can be observed repeatedly every few months or even few days. However, these multi-temporal data are generally used for database updates and change detection, but rarely be mentioned in the geometric correction of satellite imagery. Considering that the repeated observations of the same regions increase multi-baseline images from different views, the multi-temporal data are potential for obtaining more accurate object coordinate. Through experiment of the rational function model (RFM) based block adjustment of 12 multi-temporal ZiYuan-3 images without GCPs, Cao [25] demonstrated that with the increment of redundant observations of ground points, the block adjustment accuracy of multi-temporal images is better than that of mono-temporal images. Thus, we furtherly explore the positive effect of multi-coverage on the accuracy of the geometric correction, and an adaptive re-weighted block adjustment method for multi-coverage satellite stereo images is then proposed. Experiments contain a total of 722 three-line array stereo scenes of Chinese Mapping Satellite-1 images captured from December 2010 to March 2016, which cover the entire Shandong Province of China (about 158,000 km^2) nearly 10 times in space, are conducted to evaluate the adjustment accuracy of the proposed method.

II. METHOD

A. MATHEMATICAL MODEL

There are two extensively used satellite sensor models: the rigorous physical model (RPM) and the RFM. The RPM uses the collinearity equations, wherein the sensor projection center, object point, and image point are located on the same line at the instant of photography, to establish imaging geometry. Theoretically, the RPM-based block adjustment method has the highest accuracy because it represents the strict spatial relationship between image coordinates and the corresponding ground space coordinates. However, scanning lines of push-broom satellite image generally have different EOPs, leading the RPM-based geometric correction process to be complicated and time-consuming [26].

The RFM is an approximate mathematical model, whose parameters, i.e., RPC, are computed from the RPM using an object virtual grid [27]. These parameters are independent of the sensor platform and are applicable to all satellite sensors [28]. Generally, commercial satellite image providers are more willing to use RFM, such as IKONOS of Spacing imaging, QuickBird and WorldView-1/2 of DigitalGlobe, and

GeoEye-1 of GeoEye. Researchers have conducted many comparative experiments investigating the performance of RFM and RPM, and found that the RFM has higher processing efficiency, while has comparable geopositional accuracy with RPM [28]–[30].

In this study, we use the RFM with RPC, whose general expression is Equation (1), as the satellite sensor model.

$$\begin{cases} r_n = \dfrac{NumL\,(P_n, L_n, H_n)}{DenL\,(P_n, L_n, H_n)} \\ c_n = \dfrac{NumS\,(P_n, L_n, H_n)}{DenS\,(P_n, L_n, H_n)}, \end{cases} \tag{1a}$$

$$r_n = \frac{r - r_o}{r_s}, \quad c_n = \frac{c - c_o}{c_s}$$

$$P_n = = \frac{P - P_o}{P_s}, \quad L_n = \frac{L - L_o}{L_s}, \; H_n = \frac{H - H_o}{H_s} \tag{1b}$$

where (r, c) and (P, L, H) are image pixel coordinates and space coordinates, respectively. $NumL\,(P_n, L_n, H_n)$, $DenL\,(P_n, L_n, H_n)$, $NumS\,(P_n, L_n, H_n)$, and $DenS\,(P_n, L_n, H_n)$ are polynomial functions that contain 20 coefficients [27]. (r_n, c_n) and (P_n, L_n, H_n) correspond to the normalized image and object coordinates using the normalization parameters of RPC, i.e., r_o, c_o, P_o, L_o, H_o, r_s, c_s, P_s, L_s, H_s. They are generally regularized between -1 and 1 to improve the solution stability of block adjustment [28].

Due to the influence of microgravity state, environment, and temperature, the sensor placement parameters calibrated in laboratories using by RPM will change over time, thereby ultimately affecting the geopositional accuracy of stereo scenes. Many studies have demonstrated that the regenerated RFM with affine transformation can eliminate errors of stereo scenes [31]–[32],

$$\begin{cases} r_n + e_0 + e_1 r_n + e_2 c_n = \dfrac{NumL\,(P_n, L_n, H_n)}{DenL\,(P_n, L_n, H_n)} \\ c_n + f_0 + f_1 r_n + f_2 c_n = \dfrac{NumS\,(P_n, L_n, H_n)}{DenS\,(P_n, L_n, H_n)}, \end{cases} \tag{2}$$

where $(e_0, e_1, e_2, f_0, f_1, f_2)$ are the affine transformation parameters, in which (e_0, f_0) are the offset parameters that absorb most systematic errors of the RPC, and (e_1, e_2, f_1, f_2) are the drift parameters that describe the errors caused by a gyroscope drift over time [28].

B. ADAPTIVE RE-WEIGHTED BLOCK ADJUSTMENT

In the existing geometric correction methods of satellite imagery without GCPs, Equation (2) is used to establish the spatial relationship between the image and the space coordinates. The reference data such as oriented images [12], [13], DEM [14]–[16] are used as constraints, and error equations are computed through the least squares method to solve the affine transformation parameters of images. The space coordinates of the corresponding image points are forced to be consistent, and the errors in the sensor model are eliminated. The bundle adjustment, which is adopted to solve all the unknowns with a huge matrix simultaneously, requires huge memory and is not convenient for parallel processing. Therefore, it remains a challenging task for geometric correction of large-area satellite stereo scenes. Moreover, when the initial accuracies of images are uneven, such as from meters to tens of meters or even hundreds of meters, the images with poor accuracies will reduce the adjustment accuracy. In this study, we propose an adaptive re-weighted block adjustment method without GCPs based on the ''weighted virtual control points'', to overcome the above problems.

The satellite stereo scene is treated as the unit of calculation. Firstly, the space coordinates of tie points in all stereo scenes are calculated through space intersection within each stereo model. The weighted average of these space coordinates is then taken as a ''virtual control point''. Secondly, the affine transformation parameters of images are calculated separately through space resection [8] by using Equation (2). The above processes are iteratively carried out until the change of RMSE of image observations is less than the predefined threshold. The flowchart of the proposed method, which can be divided into five steps, is drawn in Fig. 1.

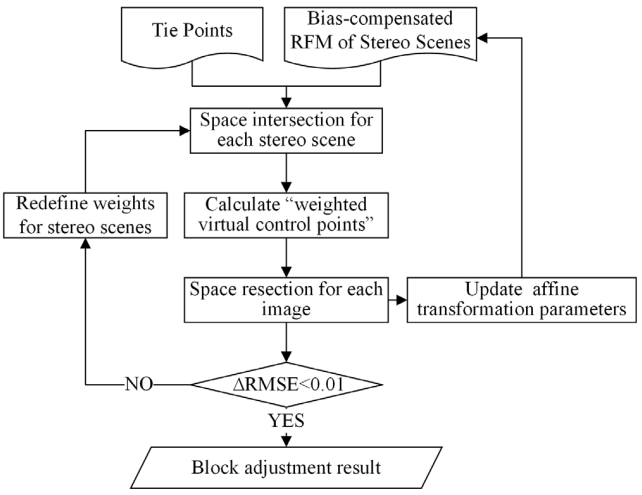

FIGURE 1. Flowchart of the proposed method.

1) SPACE INTERSECTION WITHIN EACH STEREO SCENE

The original RPC with the affine transformation parameters, whose initial values are set to zero, is used to calculate the space coordinates of the corresponding image points within each stereo scene. This calculation is conducted through space intersection based on Equation (2).

In this step, $(e_0, e_1, e_2, f_0, f_1, f_2)$ are treated as known parameters. The space coordinates (P, L, H) of the corresponding image points are unknown parameters to be solved, and the image observations (r, c) are regarded as equal weight observations. Given Equation (2) is nonlinear, it must be linearized through the Taylor formula to establish the error equation, as shown in Equation (3).

$$\boldsymbol{V} = \boldsymbol{AX} - \boldsymbol{L}, \tag{3}$$

where $\mathbf{V}$ is the vector of corrections to the image observations (r, c). $\mathbf{X}$ is the vector of the unknown space coordinates (P, L, H). $\boldsymbol{L}$ is the constant vector, and A is the coefficient matrix. The space coordinates are then solved through the least squares method.

2) CALCULATION OF "WEIGHTED VIRTUAL CONTROL POINTS"

Considering the randomness of the geopositional errors of different stereo scenes, we introduce the "virtual control point" into block adjustment instead of GCPs, which is calculated by Equation (4),

$$\tilde{\boldsymbol{X}} = \frac{\sum_{j=1}^{N} p_j \boldsymbol{X}_j}{\sum_{j=1}^{N} p_j}, \quad p_j > 0, \tag{4}$$

where $\tilde{\boldsymbol{X}}$ denotes the space coordinate of the "virtual control point", $\mathbf{X}_j$ represents the space coordinate of a tie point in stereo scene j, calculated in Step 1). N is the number of stereo scenes containing that tie point. p_j represents the weight of stereo scene j. The initial values of weights of all stereo scenes are set to 1.0.

Given that the geopositional errors of different stereo scenes are different in magnitude and direction, the space coordinates of the corresponding image points calculated in different stereo scenes are inconsistent or even contrary. To reduce the inconsistent of the space coordinates, which will cause a large error on "virtual control points", the adaptive weighting strategy is used to assign weights to the space coordinates in different stereo scenes. Detailed information will be given in step 4).

3) SPACE RESECTION FOR EACH IMAGE

Space resection for each image is then performed to solve the affine transformation parameters, namely, the unknowns $(e_0, e_1, e_2, f_0, f_1, f_2)$. All the observations (r, c) and the corresponding "virtual control points" $\tilde{\boldsymbol{X}}$ are used to construct linear equations using Equations (2). The affine transformation parameters of satellite images are solved and updated through the least squares method. The corrected value Δ of each observation and RMSE σ are then calculated. To eliminate the error caused by mismatching of tie points, an observation whose $\Delta > 3\sigma$ is considered as an outlier and furtherly deleted.

The RMSE of all observations is calculated as,

$$RMSE = \sqrt{\frac{\sum_{k=1}^{n_o} \left[\left(r_k - r_k^{'}\right)^2 + \left(c_k - c_k^{'}\right)^2 \right]}{n_o - 1}} \tag{5}$$

where (r, c) represents the image observation coordinates of tie points, $\left(r^{'}, c^{'}\right)$ represents the projection coordinates by back projection from the "weighted virtual control points" with the affine transformation parameters, n_o is the number of all observations, and k is the index number of observation.

4) REDEFINE WEIGHTS OF STEREO SCENES

In each stereo scene, the updated affine transformation parameters calculated in Step 3) are used for space intersection to compute the new space coordinates. The residual vector $\Delta \boldsymbol{X}_i$ of the space coordinate are calculated by subtracting the space coordinate in each iteration. We use the reciprocal of the $\Delta \boldsymbol{X}_{model}$ as the weight p_j of stereo scenes j in the next iteration, see Equation (6).

$$\begin{cases} p_j = \dfrac{1}{|\Delta \mathbf{X}_{model}|} = \left(\dfrac{1}{|\Delta P_{model}|}, \dfrac{1}{|\Delta L_{model}|}, \dfrac{1}{|\Delta H_{model}|} \right) \\ \Delta \mathbf{X}_{model} = (\Delta P_{model}, \Delta L_{model}, \Delta H_{model}) \\ \qquad\qquad = \sqrt{\dfrac{\sum_{i=1}^{m} (\Delta \mathbf{X}_i * \Delta \mathbf{X}_i)}{m-1}} \\ \Delta \mathbf{X}_i = \mathbf{X}_i^{new} - \mathbf{X}_i^{old} = (\Delta P_i, \Delta L_i, \Delta H_i) \end{cases} \tag{6}$$

where $\boldsymbol{X}_i^{new}$ represents the new space coordinates of tie point i. $\boldsymbol{X}_i^{old}$ denotes the space coordinates in the last iteration. m represents the number of the space coordinates in stereo scenes j. $(\Delta P_i, \Delta L_i, \Delta H_i)$, $(\Delta P_{model}, \Delta L_{model}, \Delta H_{model})$, and $\left(\frac{1}{|\Delta P_{model}|}, \frac{1}{|\Delta L_{model}|}, \frac{1}{|\Delta H_{model}|} \right)$ are the three components in three directions of the residual vector, RMSE, and weight.

The error magnitudes are different in three directions, and the differences may be in the order of magnitude, which may affect the accuracy of the result. Therefore, three weights are adaptively redefined for three directions of each stereo scene through Equation (6).

5) ITERATION

Step 2)–4) are iteratively conducted until the change of the RMSE (see Equation [5]) of all observations is less than a predefined threshold, which is set to $10e^{-2}$ in our experiments.

C. BLOCK ADJUSTMENT OF MULTI-COVERAGE SATELLITE STEREO IMAGES WITHOUT GCPS

Generally, satellite images cover the same ground region from multiple sources, multiple phases, and multi-coverage. The research and application of multi-source and multi-temporal satellite images, such as radiometric normalization [34], image registration [35], and change detection [36], are extensive. Although some works about the geometric location of multi-source data [37] have been conducted, the effect of multi-coverage on geometric correction is rarely mentioned. Thus, in this study, we explore the impact of multi-coverage on the accuracy of geometric correction.

The key of our proposed method is the "weighted virtual control point", see Equation (4). However, due to the geopositional errors of stereo scenes, the coordinate deviation will appear in the space coordinate after space intersection. The coordinate deviation $\vec{V}^N$, between "weighted virtual control point" and "real space coordinate" of tie point, can

be expressed to be weighted mathematical expectation:

$$\begin{cases} \vec{V}^N = p_1\vec{v}_1 + p_2\vec{v}_2 + \cdots + p_j\vec{v}_j \cdots + p_N\vec{v}_N \\ p_1 + p_2 + \cdots + p_j \ldots + p_N = 1, 0 < p_j < 1 \end{cases} \quad N \geq 2 \tag{7}$$

where $\vec{v}_j$ represents the coordinate deviation of the stereo scenes j, p_j is the weight of the stereo scene and represents the accuracy of the stereo scene. N represents the number of stereo scenes.

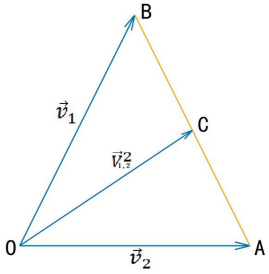

FIGURE 2. Schematic of vector addition.

In cases of mono-coverage, we can obtain Equation (8) for the tie points in the overlapping areas between stereo scenes, and the geometric representation of which in a 2D plane is illustrated in Fig. 2.

$$\begin{cases} \vec{V}^2_{1,2} = p_1\vec{v}_1 + p_2\vec{v}_2 = p_1\vec{v}_1 + (1 - p_1)\vec{v}_2 \\ p_1 + p_2 = 1,\ 0 < p_1 < 1, \end{cases} \tag{8}$$

In Fig.2, $|BC| \big/ |AB| = p_1$, $|AC| \big/ |AB| = 1 - p_1$. Obviously, regardless of the movement of the endpoint C of vector $\vec{V}^2_{1,2}$ between A and B, the magnitude of vector $\vec{V}^2$ never exceeds the maximum magnitude of $\vec{V}_1$ and $\vec{V}_2$.

$$\left|\vec{V}^2_{1,2}\right| \leq p_1 \left|\vec{V}_1\right| + (1-p_1)\left|\vec{V}_2\right| \leq max(\left|\vec{V}_1\right|, \left|\vec{V}_2\right|) \tag{9}$$

Only when $\vec{v}_1 = \vec{v}_2$, the equal sign in Equation (9) will hold. However, due to the randomness of geopositional errors in different stereo scenes, the magnitude of $\vec{V}^2$ is always smaller than the maximum magnitude of $\vec{v}_1$ and $\vec{v}_2$ in actual cases, see Equation (10). It will become smaller or even much smaller than both as the angle $\angle BOA$ increases.

$$\left|\vec{V}^2_{1,2}\right| < \max\left(|\vec{v}_1|, |\vec{v}_2|\right) \tag{10}$$

However, when an outlier occurs in $\vec{v}_1$ or $\vec{v}_2$, and no prior knowledge can be used to detect the position of the outlier, $\vec{v}_1$ and $\vec{v}_2$ will be regarded as approximately equal weight in most cases. As a result, the geopositional accuracy may be largely affected by the outlier.

In cases of multi-coverage, Equation (7) can also be expressed as Equation (11) for clarifying the relationship with mono-coverage,

$$\vec{V}^N = \frac{\sum \varphi(i,j)\vec{V}^2_{i,j}}{\sum \varphi(i,j)}, \quad i, j \in [1, N],\ i \neq j \tag{11}$$

where $\varphi(i, j)$ is a Boolean function, if the stereo scenes i and j are overlapped, then $\varphi(i, j) = 1$, otherwise $\varphi(i, j) = 0$.

Equation (11) shows that the coordinate deviation of multi-coverage case can be simply regarded as the expected value of the coordinate deviations of several mono-coverage cases. Different from the mono-coverage, multi-coverage can provide redundant observations, which can eliminate errors between stereo scenes better and is useful for locating outliers. Moreover, the adaptive weighted strategy can effectively suppress the outliers improving the geopositional accuracy of multi-coverage. However, it should be noted that, since the accuracy of block adjustment without GCPs depends on the size and distribution of the geopositional errors of the stereo scenes, it may not increase when only a few stereo scenes are used.

III. EXPERIMENTS AND RESULTS

The experimental dataset consists of 2166 images of Chinese Mapping Satellite-1 images, which is the first generation of 3D mapping satellite launched by China in August 2010. The satellite is designed for scientific research, land surveying and mapping, it carries three stereo mapping cameras (forward, nadir, and backward cameras for capturing three-line array stereo image), one high resolution camera, and one multispectral camera [38]. The ground sampling distances of the three-line array stereo images are 5 m, and the ground range of the standard scene is approximately 60 km × 60 km (12000 pixels × 12000 pixels). The experimental area covers the whole Shandong Province, China, with a longitude range of E114° − E123° and a latitude range of N33° − N39°. The 2166 images collected from December 2010 to March 2016, forming 722 three-line array stereo scenes (each stereo scene consists of forward/nadir/backward images), cover the experimental area for nearly 10 times. Well-distributed 100 ground check points are used to assess the adjustment accuracy. The distributions of images and ground check points are shown in Fig. 3(a). A total of 5,494,988 tie points are extracted by image matching. It is worth noting that only 530 stereo scenes cover the ground check points. Fig. 3(b) displays the distribution of coverage times of stereo scenes, by accumulating the number of times that the ground grids matrix intersecting with the footprints of 722 stereo scenes. The coverage times increase while the color varies from blue to red.

Several experiments are designed to evaluate the proposed method. Firstly, error distribution of all the 722 stereo scenes is discussed in A. Secondly, to verify the feasibility of the proposed method, the geopositional accuracies of stereo scenes before and after block adjustment are compared in B. Then, a series of experiments about multi-coverage and mono-coverage are used to validate the effect of multi-coverage on block adjustments without GCPs in C. Finally, an exploration about the relationship between the coverage times and the geopositional accuracy of block adjustment without GCPs is presented in D.

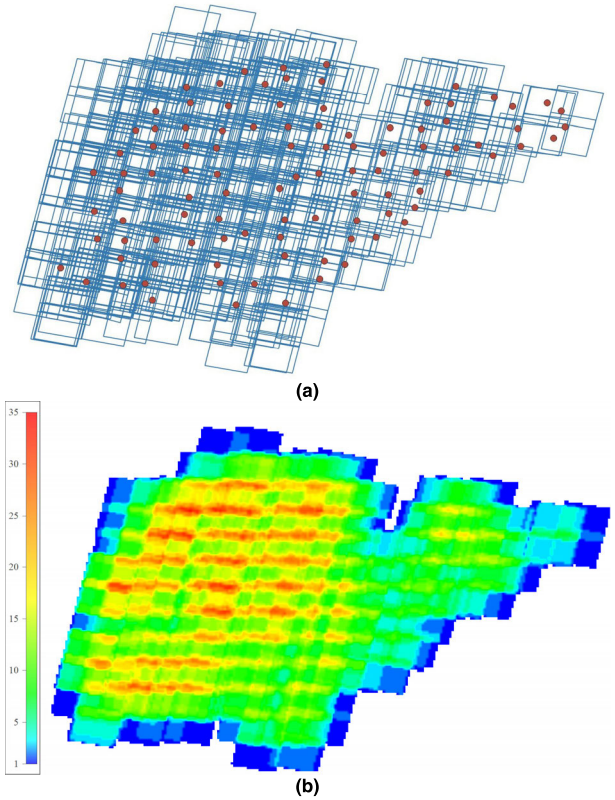

FIGURE 3. The experimental dataset of Chinese mapping Satellite-1 over Shandong province of China. (a) Footprints of images and ground check points, (b). Distribution of coverage times of stereo scenes.

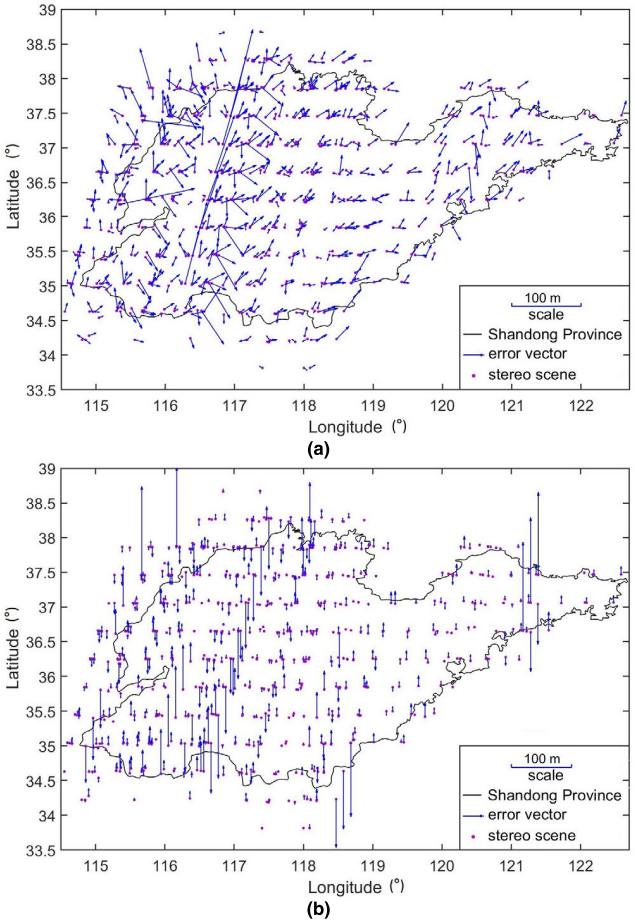

FIGURE 4. Direct geopositional errors of the 722 stereo scenes in the Shandong test area. (a) Horizontal errors (b) vertical errors.

A. ASSESSMENT OF DIRECT GEOPOSITIONAL ACCURACY

Considering that not all of the 722 stereo scenes have ground check points, directly assessing their direct geopositional accuracies is infeasible. Thus, an indirect assessment method is adopted. Firstly, block adjustment using all of the 100 ground check points as control is performed, and the adjusted space coordinates of tie points are considered as the real space coordinates. Secondly, the initial coordinates of tie points in every stereo scene are calculated through space intersection using the original RPCs. The difference between the initial and the adjusted coordinates of each tie point is then calculated, which is treated as the direct geopositional accuracy of the tie point. And the direct geopositional accuracy (error) of a stereo scene is defined as the average of the differences of all the tie points in it. The direct geopositional accuracies of the 722 stereo scenes are exhibited in Fig. 4 and Fig. 5.

Figs. 4(a) and 4(b) display the direct geopositional accuracies in the horizontal and vertical directions, respectively. The purple points present the central positions of the stereo scenes, and the blue arrows denote the error vectors. The magnitudes and directions of the errors among stereo scenes are inconsistent and random, especially for stereo scenes in different tracks. However, the horizontal errors of the same-track stereo scenes are similar in magnitude and direction, which indicates a strong systematicity, as depicted in Fig. 5(a). Although the vertical error vectors of the same-track stereo scenes do not show systematic characteristics as a whole (Fig. 5(b)), these vectors are similar to the magnitude and direction in the local region of the same tracks.

B. BLOCK ADJUSTMENT WITHOUT GCPS

Block adjustment without GCPs is then performed. The residual errors of tie points, which use the adjusted space coordinates calculated by block adjustment with GCPs as the real space coordinates, are also calculated for each stereo scene. Moreover, the RMSE of tie points in each stereo scene is defined as the geopositional accuracy of the block adjustment without GCPs for a stereo scene. Fig. 6 plots the comparison of geopositional accuracies of stereo scenes before and after block adjustment without GCPs.

The blue and red line represent direct geopositional accuracies of stereo scenes before block adjustment and after block adjustment without GCPs, respectively. The blue line in Fig. 6 illustrates that the initial RPCs of images contain varying degrees of errors in the X-, Y-, and Z-directions, especially in a few stereo scenes with large errors, which will significantly affect the results of geometric positioning. On the contrary, the red line has a small fluctuation range, and

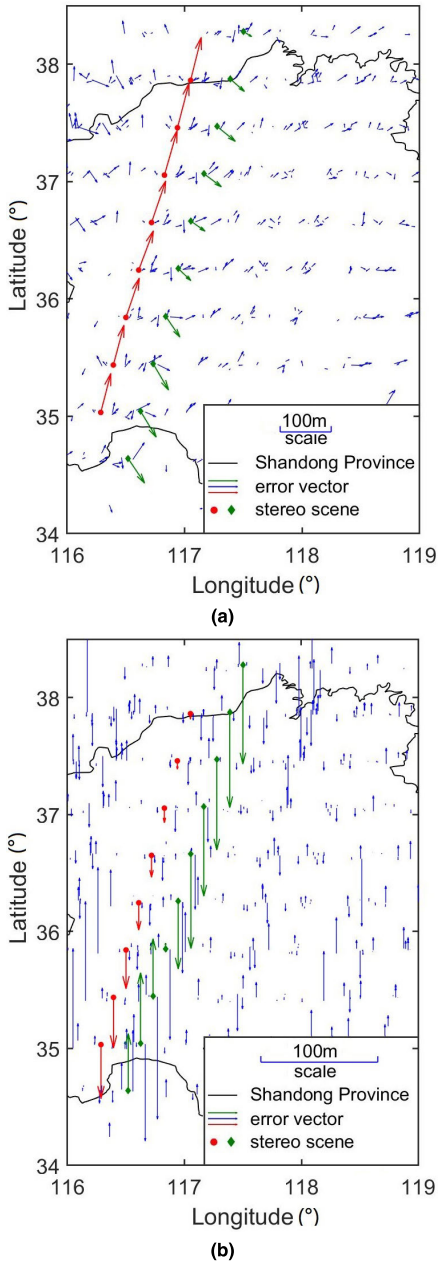

FIGURE 5. Direct geopositional errors of stereo scenes in the sub-region (E116-E117.5E114° – E123°, N34.5-N38), red circles and green diamonds represent two same-track stereo scenes. (a) Horizontal errors (b) vertical errors.

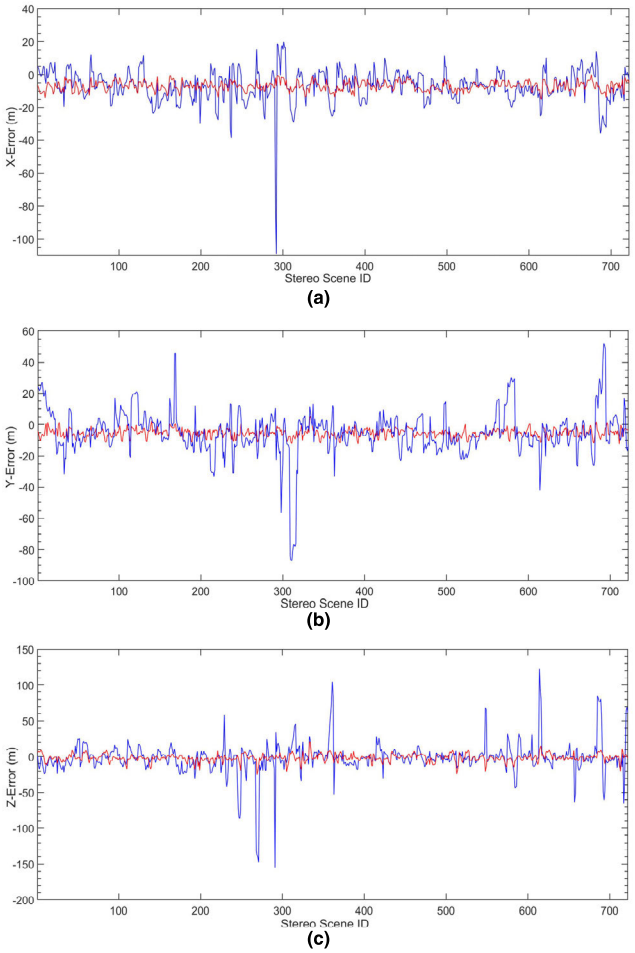

FIGURE 6. Geopositional accuracies of stereo scenes before and after block adjustment without GCPs in the (a) X, (b) Y, and (c) Z directions.

TABLE 1. Geopositional accuracies of the initial and the adjusted stereo scenes.

Experiments		Max (m)	Min (m)	RMSE (m)
Before BA	XY	111.35	1.11	19.59
	Z	154.55	0.02	22.38
After BA	XY	18.92	0.48	9.49
	Z	25.30	0.00	5.64

'BA' represents block adjustment without GCPs.

the center of gravity is significantly close to 0. It indicates the reduction of errors in most stereo scenes after geometric correction through the proposed method, especially for the stereo scenes with large errors. The red and blue lines randomly fluctuated around the same negative values (about −8 m in X, −5 m in Y, and −3 m in Z) in the X-, Y-, and Z-directions, thus denoting that a consistent systematic error exists in the initial RFMs of all stereo scenes. Moreover, these systematic errors are retained after geometric correction because no control data are involved in the block adjustment to constraint the result.

We also count the maximum (Max), minimum (Min), and RMSE of the geopositional errors of all stereo scenes in the horizontal and vertical directions, as presented in Tab. 1. Tab. 1 displays that the direct geopositional accuracies of stereo scenes are poor, and their horizontal and vertical RMSEs are approximately 4 pixels and 4.5 pixels, respectively. The maximum error is more than 30 pixels. The geopositional accuracies of the stereo scenes have improved significantly after applying the proposed method, especially the reduction in error in the vertical direction from 4.5 pixels to 1.2 pixels. The changes in the maximum, minimum, and RMSE show that large differences among all stereo scenes are reduced significantly, and the stereo scenes with large errors are well-corrected. The result indicates that the proposed method can effectively eliminate the errors in the initial stereo

TABLE 2. Geopositional accuracies for 530 stereo scenes covering GCPS.

Experiments		Max (m)	Min (m)	Mean (m)	Std (m)	RMSE (m)
Before BA	XY	123.34	1.26	16.55	13.04	21.08
	Z	150.27	0.05	12.97	19.53	23.45
After BA	XY	69.15	0.14	10.74	4.67	11.72
	Z	96.95	0.03	5.81	6.23	8.52

'BA' represents block adjustment without GCPs.

scenes and the re-weighted strategy can effectively suppress the influence of the stereo scene with a large error.

To furtherly evaluate the proposed method, the geopositional accuracies before and after block adjustment of 530 stereo scenes, which covering several GCPs, are also counted using GCPs as reference. Firstly, the space coordinates of GCPs are obtained using the space intersection for each stereo scene. Then the deviation from the real space coordinates is calculated. Finally, the mean of deviations of the covered GCPs is taken as the geopositional accuracy for each stereo scene. And statistical results of accuracies for the 530 stereo scenes are showed in Tab. 2.

The results in Tab. 2 are similar to those in Tab. 1, which in turn indicates that it is reliable to evaluate the geopositional accuracies of stereo scenes before and after block adjustment by using the result of block adjustment with 100 GCPs as reference. Especially, the standard variance of all deviations is reduced to less than one-third of the initial stereo scenes, which demonstrates that the proposed method can effectively suppress large errors and make the errors more concentrated.

C. MONO-COVERAGE EXPERIMENTS

We also conduct three comparison experiments to verify that multi-coverage can effectively improve the accuracy of block adjustment. Three groups of mono-coverage stereo scenes are selected from the dataset. The selection is under the constraint of covering the same range as the original dataset as much as possible. Moreover, the stereo scenes of the three groups are not duplicated, and each group covers all of the 100 ground check points. The selected three groups consist of 90, 95, and 95 stereo scenes, respectively. After block adjustment without GCPs, the accuracies of multi- and mono-coverage experiments are evaluated by counting the mean error, standard variance, and RMSE of the ground check points. The results are presented in Tab. 3 and Fig. 7.

Table 3 summarizes that the horizontal accuracies of the three mono-coverage groups are approximately 3 pixels. However, the vertical accuracies of the three groups vary

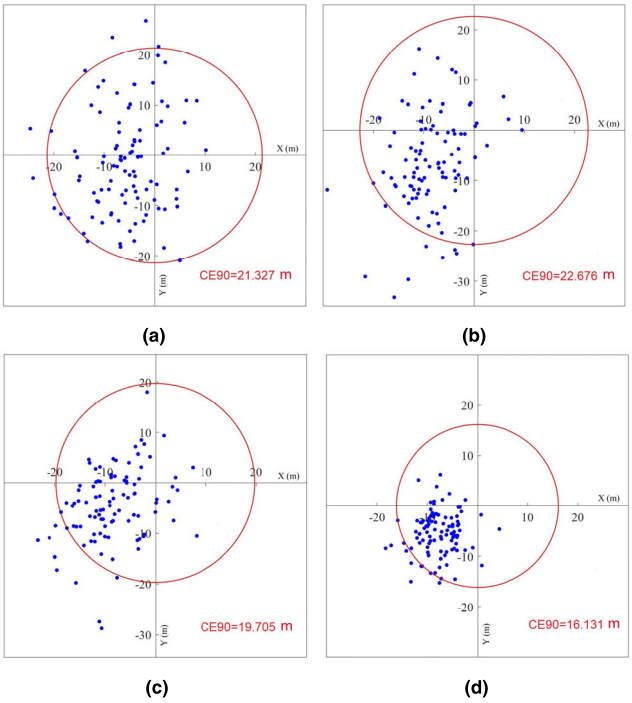

FIGURE 7. Horizontal error distribution of the different groups. (a) Mono-coverage1 group. (b) Mono-coverage2 group. (c) Mono-coverage3 group. (d) Multi-coverage group.

significantly. For example, the vertical RMSE of the first group is nearly twice than that of the third group.

The three mono-coverage groups combined with Fig. 4 demonstrate that the weak regularity of vertical errors leads to its instability for the mono-coverage block adjustment without GCPs. The RMSE of the multi-coverage experiment is within 2 pixels in the X-, Y-, and Z-directions, which is smaller than that of the three mono-coverage groups. The vertical accuracy is significantly improved because the multi-coverage can increase the intersection angle among the stereo scenes. This result indicates that multi-coverage can effectively improve geopositional accuracy. Moreover, the mean errors of the four experiments are less than 0. The systematic errors remain in all stereo scenes because of the absence of real control data.

Fig. 7 plots the horizontal error distributions of 100 checkpoints in the three mono-coverage groups and the multi-coverage experiment. The red circle in the figures refers to CE90 (circular error with a 90% confidence). The CE90 circle is much smaller in multi-coverage than in the three mono-coverage. This result indicates that multi-coverage can

TABLE 3. Accuracy of block adjustment without GCPS.

Data groups	RMSE (m)				Mean Error (m)			Standard Variance (m)		
	X	Y	XY	Z	X	Y	Z	X	Y	Z
Mono1 (90)	8.97	10.35	13.69	29.27	−5.69	−1.32	−10.50	6.93	10.27	27.34
Mono2 (95)	10.36	12.22	16.02	21.47	−8.43	−7.08	−1.85	6.02	9.96	21.39
Mono3 (95)	11.34	8.86	14.39	16.39	−8.80	−4.30	−2.76	7.15	7.74	16.16
Multi (722)	8.68	6.90	11.09	8.47	−7.84	−5.39	−3.08	3.73	4.31	7.89

achieve higher geopositional accuracy than mono-coverage. Moreover, the errors of the multi-coverage experiment are concentrated, as reflected by the standard variance of errors in Tab. 2. It indicates that multi-coverage can constraint the results of local regions well, thereby making the accuracy of each region increasingly uniform.

D. THE RELATIONSHIP BETWEEN THE OBSERVATION TIMES AND THE GEOPOSITIONAL ACCURACY

The experiment C has proved that the multi-coverage can provide redundant observations to reduce the geopositional error. However, the relationship between the coverage times and the geopositional accuracy is ignored by present studies about geometric positioning for satellite imagery [25]. In this section, an experiment on the quantitative relationship between the coverage times and the geopositional accuracy of block adjustment without GCPs is explored.

The experiments start from the block adjustment without GCPs of a mono-coverage case, then the stereo scenes with uniform distribution within the experimental range are added group by group, until all of the 722 stereo scenes are added into the experiment. Because 722 stereo scenes of Shandong dataset are not evenly distributed, and each sub-dataset is extracted according to the principle of covering the experimental area as much as possible with the least coverage times, so the coverage times and the number of stereo scenes in each sub-dataset are not equal. Therefore, 15 experiments are finally taken. In each experiment, the coverage times and the RSME of 100 ground check points are accounted, which is shown in Fig. 8.

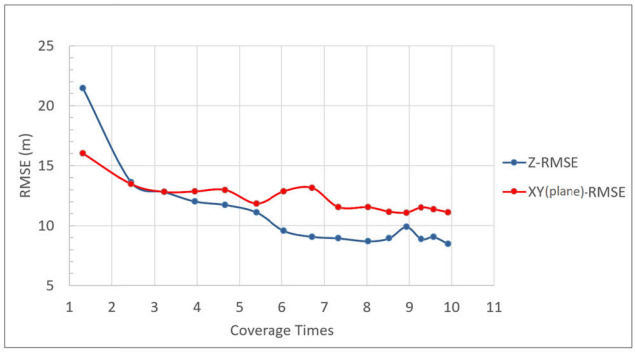

FIGURE 8. The relationship between the coverage times and the geopositional accuracy of block adjustment without GCPs. XY (plane)-RMSE: RMSE in the horizontal direction. Z-RMSE: RMSE in the vertical direction.

Fig. 8 shows that the geopositional accuracy of block adjustments without GCPs presents an increasing trend as the coverage times increases, which verifies that multi-coverage can effectively improve geopositional accuracy. The decline rate of RMSE gradually becomes slower as the coverage times increases. Especially, after reaching 7 coverage times, both of the two RMSE curves gradually start to be approximately parallel to the x-axis. It is worth noting that the Z-RMSE drops faster than XY-RMSE and enters the stable status more quickly, which indicates that the increase of coverage times can better improve the accuracy in the vertical direction.

IV. CONCLUSION

In this study, we proposed an adaptive re-weighted block adjustment method without GCPs for satellite stereo images based on the bias-compensated rational function model with affine transformation parameters. The ''weighted virtual control points'' was introduced as the constraint of the block adjustment, and the re-weighted approach was used to reduce the adverse effect of the stereo scene with a large error on the overall adjustment accuracy. The positive influence of multi-coverage on improving the accuracy of adjustment without GCPs was discussed, and the quantitative relationship between the coverage times of stereo images and the final accuracy of block adjustment was also investigated. The experiment with 722 stereo scenes of Chinese Mapping Satellite-1 images, which cover the entire Shandong Province of China (about 158,000 km^2) nearly 10 times in space, achieved an accuracy within 2 pixels in the X-, Y-, and Z-directions. These experiments lead to the following conclusions.

(1) The proposed method of adaptive re-weighted block adjustment without GCPs can effectively eliminate errors in satellite stereo images.

(2) The participation of multi-coverage satellite stereo images, which include redundant observations, can significantly improve the accuracy of block adjustment without GCPs, more specifically, from 13.69-16.02 m to 11.09 m in the horizontal direction, and from 16.39-29.27 m to 8.47 m in the vertical direction, for the experimental dataset in this study.

(3) The final accuracy of block adjustments without GCPs presents an increasing trend as the coverage times of stereo images increases, and will keep stable when the coverage times reaches to a certain number, i.e., 7.4 times in this study.

REFERENCES

[1] L. Zhang, J. Zhang, X. Chen, and H. An, ''Block-adjustment with SPOT-5 imagery and sparse GCPs based on RFM,'' *Acta Geodaetica Cartographica Sinica*, vol. 38, no. 4, pp. 302–310, Aug. 2009.

[2] H. Fang, B. Hu, Z. Yu, H. Xu, C. He, A. Li, and Y. Liu, ''Semi-automatic geometric correction of airborne hyperspectral push-broom images using ground control points and linear features,'' *Int. J. Remote Sens.*, vol. 39, no. 2, pp. 4115–4129, Jun. 2018.

[3] R. R. Jensen, A. J. Hardin, P. J. Hardin, and J. R. Jensen, ''A new method to correct pushbroom hyperspectral data using linear features and ground control points,'' *GISci. Remote Sens.*, vol. 43, no. 3, pp. 416–431, Jul. 2011.

[4] H. Babapour, M. Mokhtarzade, and M. J. V. Zoej, ''A novel post-calibration method for digital cameras using image linear features,'' *Int. J. Remote Sens.*, vol. 38, nos. 8–10, pp. 2698–2716, May 2016.

[5] J. M. Junior and A. M. G. Tommaselli, ''Exterior orientation of CBERS-2B imagery using multi-feature control and orbital data,'' *ISPRS J. Photogram. Remote Sens.*, vol. 79, pp. 219–225, May 2013.

[6] F. Rottensteiner, T. Weser, A. Lewis, and C. S. Fraser, ''A strip adjustment approach for precise georeferencing of alos optical imagery,'' *IEEE Trans. Geosci. Remote Sens.*, vol. 47, no. 12, pp. 4083–4091, Dec. 2009.

[7] O. Mutluoglu, M. Yakar, and H. M. Yilmaz, ''Investigation of effect of the number of ground control points and distribution on adjustment at WorldView-2 Stereo image,'' *Int. J. Appl. Math., Electron. Comput.*, vol. 3, no. 1, pp. 37–41, 2015.

[8] B. G. Das, "A mathematical approach to problems in photogrammetry," *Empire Survey Rev.*, vol. 10, no. 73, pp. 131–137, 1949.
[9] P. Cheng and C. Chaapel. (2016). *Using WorldView-1 Stereo Data With or Without Ground Control Points—Automatic DEM Generation*. Accessed: Oct. 28, 2019. [Online]. Available: https://www.researchgate.net/publication/263272412 >
[10] Y. Ming, C. J. Chen, S. H. Yu, and X. Zhang, "Geolocation accuracy analysis of multi-strip WorldView satellite imagery," *Sci. Surveying Mapping*, vol. 38, no. 1, pp. 160–162, Jan. 2013.
[11] Z. Zhang and P. Tao, "An overview on 'cloud control,' photogram. Big data era," *Acta Geodaetica Cartographica Sinica*, vol. 1, no. 2, pp. 1238–1248, 2017.
[12] Z. Ma, X. Wu, L. Yan, and Z. Xu, "Geometric positioning for satellite imagery without ground control points by exploiting repeated observation," *Sensors*, vol. 17, no. 2, pp. 240–256, Jan. 2017.
[13] Z. Ma, W. Song, J. Deng, J. Wang, and C. Cui, "A rational function model based geo-positioning method for satellite images without using ground control points," *Remote Sens.*, vol. 10, no. 2, pp. 182–201, Jan. 2018.
[14] J. Jeong and T. Kim, "The use of existing global elevation dataset for absolute orientation of high resolution image without GCPs," in *Proc. Int. Arch. Photogramm., Remote Sens. Spatial Inf. Sci.*, 2012, pp. 287–290.
[15] H. Lee, B. Park, and K. Ahn, "Accuracy improvement of KOMPSAT-3 DEM using previous DEMs without ground control points," *J. Korean Soc. Surveying Geodesy Photogram. Cartography*, vol. 35, no. 2, pp. 241–248, Aug. 2017.
[16] T. Wang, G. Zhang, D. Li, W. Jiang, X. Tang, and X. Liu, "Comparison between plane and stereo block adjustment for zy-3 satellite images," *Acta Geodaetica Cartographica Sinica*, vol. 44, no. 2, pp. 389–395, Apr. 2014.
[17] M. Gianinetto and M. Scaioni, "Automated geometric correction of high-resolution pushbroom satellite data," *Photogramm. Eng. Remote Sens.*, vol. 74, no. 1, pp. 107–116, Jan. 2008.
[18] P. Tao, L. Lu, Y. Zhang, B. Xu, and S. Zou, "On-orbit geometric calibration of the panchromatic/multispectral camera of the ZY-1 02C satellite based on public geographic data," *Photogramm. Eng. Remote Sens.*, vol. 80, no. 6, pp. 505–517, Jun. 2014.
[19] T. Toutin, C. V. Schmitt, and H. Wang, "Impact of no GCP on elevation extraction from worldview stereo data," *ISPRS J. Photogramm. Remote Sens.*, vol. 72, pp. 73–79, Aug. 2012.
[20] S. Tang, B. Wu, and Q. Zhu, "Combined adjustment of multi-resolution satellite imagery for improved geo-positioning accuracy," *ISPRS J. Photogramm. Remote Sens.*, vol. 114, pp. 125–136, Apr. 2016.
[21] Y. Jiang, L. Xu, and X. Tao, "Mathematical modeling and accuracy testing of WorldView-2 Level-1B stereo pairs without ground control points," *Remote Sens.*, vol. 9, no. 7, p. 737, Jul. 2017.
[22] R. Mumtaz, P. L. Palmer, and M. M. Waqar, "Georeferencing of UK DMC stereo-images without ground control points by exploiting geometric distortions," *Int. J. Remote Sens.*, vol. 35, no. 6, pp. 2136–2169, Mar. 2014.
[23] Y. Zhang, M. Zheng, X. Xiong, and J. Xiong, "Multistrip bundle block adjustment of ZY-3 satellite imagery by rigorous sensor model without ground control point," *IEEE Geosci. Remote Sens. Lett.*, vol. 12, no. 4, pp. 865–869, Apr. 2014.
[24] B. Yang, M. Wang, W. Xu, D. Li, J. Gong, and Y. Pi, "Large-scale block adjustment without use of ground control points based on the compensation of geometric calibration for ZY-3 images," *ISPRS J. Photogram. Remote Sens.*, vol. 134, pp. 1–14, Dec. 2017.
[25] Cao, J, "Block Adjustment of ZY-3 Multi-Temporal Images Without Ground Control Points," in *Proc. 2nd Int. Conf. Frontiers Sensors Technol. (ICFST)*, Apr. 2017, pp. 251–255.
[26] A. Habib, S. W. Shin, K. Kim, C. Kim, K. I. Bang, E. M. Kim, and D. C. Lee, "Comprehensive analysis of sensor modeling alternatives for high resolution imaging satellites," *Photogramm. Eng. Remote Sens.*, vol. 73, no. 2, pp. 1241–1251, Nov. 2007.
[27] C. V. Tao and Y. Hu, "A comprehensive study of the rational function model for photogrammetric processing," *Photogramm. Eng. Remote Sens.*, vol. 1, no. 2, pp. 1347–1357, Dec. 2001.
[28] J. Grodecki and G. Dial, "Block adjustment of high-resolution satellite images described by rational polynomials," *Photogramm. Eng. Remote Sens.*, vol. 69, no. 2, pp. 59–68, Jan. 2003.
[29] X. Yang, "Accuracy of rational function approximation in photogrammetry," in *Proc. ASPRS Annu. Conf.*, 2000, pp. 22–26.
[30] L. Zhang, T. Balz, and M. Liao, "Satellite SAR geocoding with refined RPC model," *ISPRS J. Photogram. Remote Sens.*, vol. 69, pp. 37–49, Apr. 2012.
[31] K. S. Sekhar, A. S. Kumar, and V. K. Dadhwal, "Geocoding RISAT-1 MRS images using bias-compensated RPC models," *Int. J. Remote Sens.*, vol. 18, no. 2, pp. 7303–7315, Oct. 2014.
[32] C. S. Fraser and H. B. Hanley, "Bias-compensated RPCs for sensor orientation of high-resolution satellite imagery," *Photogramm. Eng. Remote Sens.*, vol. 71, no. 2, pp. 909–915, Aug. 2005.
[33] J. Oh and C. Lee, "Automated bias-compensation of rational polynomial coefficients of high resolution satellite imagery based on topographic maps," *ISPRS J. Photogram. Remote Sens.*, vol. 100, pp. 14–22, Feb. 2015.
[34] C. Hu and P. Tang, "Automatic algorithm for relative radiometric normalization of data obtained from Landsat TM and HJ-1A/B charge-coupled device sensors," *J. Appl. Remote Sens.*, vol. 6, no. 1, 2012, Art. no. 063509.
[35] I. N. F. Aicardi, M. Gerke, and A. M. Lingua, "An image-based approach for the co-registration of multi-temporal UAV image datasets," *Remote Sens.*, vol. 1, no. 8, no. 9, pp. 779–798, 2016.
[36] C. Wu, L. Zhang, and L. Zhang, "A scene change detection framework for multi-temporal very high resolution remote sensing images," *Signal Process.*, vol. 124, pp. 184–197, Jul. 2015.
[37] G. Zhang and X. Tang, "Block adjustment from multi-sensor imagery," in *Proc. 12th Conf. Int. Assoc. Math. Geology*, Beijing, China, 2007, pp. 498–501.
[38] R. Wang, X. Hu, X. Wang, and J. Yang, "The construction and application of Mapping Satellite-1 engineering," *J. Remote Sens.*, vol. 16, no. 1, pp. 2–5, 2012.

KUNBO LIU received the B.S. and M.S. degrees from the School of Remote Sensing and Information Engineering, Wuhan University, Wuhan, China, in 2013 and 2015, respectively, where he is currently pursuing the Ph.D. degree with the School of Remote Sensing and Information Engineering. His current research interests include geometrical and radiometric processing of satellite images.

PENGJIE TAO received the B.S. and Ph.D. degrees from the School of Remote Sensing and Information Engineering, Wuhan University, Wuhan, China, in 2008 and 2016, respectively, where he is currently an Associate Research Fellow with the School of Remote Sensing and Information Engineering. His research interests include satellite images photogrammetry, registration of optical images and LiDAR points, multi-view images, and three-dimensional reconstruction.

KAI TAN received the B.S. degree from the School of Geodesy and Geomatics, Wuhan University, Wuhan, China, in 2011, and the Ph.D. degree from the College of Surveying and Geo-Informatics, Tongji University, Shanghai, China, in 2017.

He is currently a Postdoctoral and a Research Associate with the State Key Laboratory of Estuarine and Coastal Research, East China Normal University, Shanghai. His research interests include LiDAR data processing, LiDAR intensity data correction, and 3-D modeling.

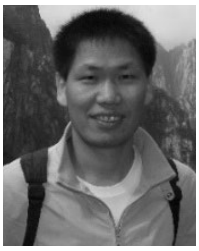

YANSONG DUAN was born in 1975. He received the M.S. and Ph.D. degrees from Wuhan University, Wuhan, China, in 2009 and 2016, respectively, where he is currently a Teacher with the School of Remote Sensing and Information Engineering. His research interests include photogrammetry, image matching, 3-D city reconstruction, computer vision, and high-performance computing with GPU.

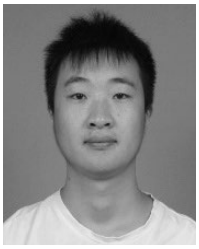

JIANAN HE received the B.S. degree from Wuhan University, Wuhan, China, in 2014, where he is currently pursuing the Ph.D. degree with the School of Remote Sensing and Information Engineering.

His research interests include image matching, aerial photogrammetry, orthoimage mosaicing, and parallel computing.

XIANGYONG LUO received the B.S. and M.S. degrees from the School of Remote Sensing and Information Engineering, Wuhan University, Wuhan, China, in 2004 and 2006, respectively.

He is currently with the Key Laboratory for Aerial Remote Sensing Technology of Ministry of Natural Resources of the People's Republic of China. His current research interests include Research and Development of photogrammetry software system, remote sensing data processing based on high-performance computing, big data, and cloud computing.